Article:
Yang, J, Sebilleau, F and Hewitt, GF (2018) The role of disturbance waves in nucleate boiling in annular flow. International Journal of Heat and Mass Transfer, 116. pp. 609-616. ISSN 0017-9310

https://doi.org/10.1016/j.ijheatmasstransfer.2017.08.044

The Role of Disturbance Waves in Nucleate Boiling in Annular Flow

Junfeng Yang, Frederic Sebilleau and Geoffrey F. Hewitt

Department of Chemical Engineering, Imperial College London

Email Address: jungfeng.yang@imperial.ac.uk

Telephone: +44(0)744 333 1919

Abstract: In annular two-phase gas-liquid flow, the liquid film on the wall consists of relatively quiescent *substrate* regions which are traversed by large amplitude, high velocity waves known as *disturbance waves*. The turbulent disturbance wave regions have relatively high average heat transfer coefficients (low average wall temperatures) compared to the (probably laminar) substrate regions. Nevertheless, there is evidence that nucleate boiling (necessitating a higher wall temperature) occurs first in the wave regions. This paper explores the hypothesis that wall temperature fluctuations due to turbulence in the disturbance waves are of sufficient magnitude to give localized triggering of nucleation sites and hence nucleate boiling. This hypothesis was explored using Computational Fluid Dynamics (CFD). The turbulence was modelled using wall-resolved LES. The results lend weight to the hypothesis that the nucleate boiling observed in disturbance waves is due to transient local high temperatures induced by the turbulence.

Keywords: disturbance wave, heat transfer, annular flow, large eddy simulation.

Nomenclature

Acronyms

CFD	Computational Fluid Dynamics
LES	Large Eddy Simulation
RANS	Reynolds-Averaged Navier-Stokes
WLES	Wall-Resolved Large Eddy Simulation
SIMPLE	Semi-implicit Method for Pressure-linked Equation
HTC	Heat Transfer Coefficient
RMS	Root-Mean-Square

Subscript

m, n	the index of velocity probe
i, j, l	the vector components in the *i*-th, *j*-th and *l*-th directions
G	gas phase
Sub	
Sat	
Peak	

Symbols

Ls, Cs	model constant
Cp	heat capacity
g	gravitational acceleration (m/s^2)
p	pressure (Pascal)
T	temperature (K)
μ	molecular viscosity
μ_t	sub-grid scale turbulent viscosity
ρ	density

ρ_{mm}	correlation coefficient
λ	thermal conductivity
τ_i	interfacial shear stress
τ_{ij}	sub-grid scale stress
σ	viscous stress tensor
h_s	sensible enthalpy
u	velocity, m/s
S	rate-of-strain tensor
Re	Reynolds number (-)
Pr_t	sub-grid scale Prandtl number (-)
Δ	local grid size
r, θ, z	parameters of cylindrical coordinates
t	time
x, y, z	the vector components in the x-th, y-th and z-th directions
f_i	interfacial friction factor
D	pipe diameter
δ	the local film thickness
$k_{s,d}$	the equivalent sand roughness
Cr	Courant number
Δt	the maximum time step size
Δl	the dimension of the grid cell at each location
U	the average linear velocity
Y^+	

Nomenclature

Acronyms

HFC	hydrofluorocarbon
HFO	hydrofluoroolefin
WHR	waste heat recovery
ORC	organic Rankine cycle
HX	heat exchanger
BPHX	brazed plate heat exchanger
TC	thermocouple
PT	pressure transmitter
DPS	differential pressure sensor
CFM	Coriolis flow meter
TFM	turbine flow meter
MFM	magnetic flow meter
AV	automatic valve
MV	manual valve
R	refrigerant

Subscripts

su	supply
ex	exit
wf	working fluid
hf	hot fluid
wat	water
eva	evaporator
meas	measured
m	mean
p	plate
ch	channel
v	saturated vapor
l	saturated liquid
vap	vaporization

Symbols

p	pressure (bar)
T	temperature (°C)
ρ	density (kg m^{-3})
μ	viscosity (Pa s)
k	thermal conductivity (W m^{-1} k^{-1})
h	specific enthalpy (J kg^{-1})
α	fluid heat transfer coeff. (W m^{-2} k^{-1})
U	overall heat transfer coeff. (W m^{-2} k^{-1})
$\dot{Q}$	thermal power (W)
$\dot{q}$	thermal flux (W m^{-2})
$\dot{m}$	mass flow rate (kg s^{-1})
G	mass flux (kg s^{-1} m^{-2})
c_p	specific heat capacity (J kg^{-1} K^{-1})
X	vapor quality (–)
l_p	wall thickness (m)
d_h	hydraulic diameter (m)
Re	Reynolds number (–)
Pr	Prandtl number (–)
We	Weber number (–)
Bo	boiling number (–)
Bd	Bond number (–)
Nu	Nusselt number (–)

1. Introduction

Annular two-phase gas-liquid (or vapour-liquid) flow occurs in a wide range of industrial equipment (boilers, condensers, pipelines etc.) and is characterized by the presence of a thin, wavy liquid film driven along the wall by the shear force exerted by the gas (or vapor) phase in the core (Hewitt and Hall-Taylor [1]). The film/core interface is covered by a complex pattern of waves (Hall-Taylor et al, [2]). These waves are typically of two main types, namely *ripples* which are of small amplitude and cover the whole film surface and *disturbance waves.* The disturbance waves have amplitude of the order of 5-6 times the mean film thickness and travel along the interface at much higher velocity than do the ripples. Calculation of the mean heat transfer coefficient in annular flow based on mean film thickness and mean interfacial shear stress gives rise to a gross over-prediction of the coefficient [1] and it is evident that the intermittent nature of annular flow (and in particular the influence of disturbance waves) needs to be taken into account.

Detailed measurements of the shapes of disturbance waves were carried out by Hewitt and Nichols [3] using a fluorescence method and Jayanti and Hewitt [4] used this data to specify the geometry of a typical disturbance wave. Jayanti and Hewitt then used computational fluid dynamics (CFD) methods to determine the temperature distribution in the disturbance waves and in the substrate regions between the waves. It was found that the wave regions were turbulent and had a high heat transfer coefficient whereas the substrate regions were laminar and had a low coefficient. Moreover, the mean predicted heat transfer coefficient was in much better agreement with measured values than were values calculated based on the *mean* film thickness and shear stress.

The calculations by Jayanti and Hewitt [4] suggest that the wall temperature (for a given heat flux) would *fall* in the disturbance wave region and *rise again* when the disturbance wave passed. This would normally mean that the likelihood of nucleate boiling (i.e. evaporation by the formation of bubbles at the surface) was greater in the substrate region. However, this conclusion is contradicted by more recent experiments by Barbosa et al [5] who observed that nucleate boiling occurred in the disturbance wave itself and was suppressed in the substrate regions. Possible explanations of this behavior include the following:

(1) Reduction of pressure in the wave region. Because the core gas accelerates in order to flow over the wave, this implies a reduction in pressure in the wave region. One may associate this to a reduction in saturation temperature and an increased propensity to nucleation. Approximate calculations on the pressure change in passing from the substrate region to the wave peak indicate a value of the order of 500 Pa for the present results. This corresponds to a small fraction of a degree in saturation temperature and so this explanation is unlikely to account for the transient increase in intensity of nucleation which is observed

It should also be recognized that the *shape* of the gas velocity profile changes as the gas flows from the relatively smooth substrate region to the rough wave region (Jayanti and Hewitt [7], Jayanti et al [8]) this would increase the pressure change associated with the wave region but, even accounting for this additional complexity, the pressure change would give rise only to a small change in saturation

temperature. Thus, reduction of pressure (and hence saturation temperature, is unlikely to be the cause of nucleation events observed by Barbosa et al [5].

(2) Bubble entrainment in waves. The highly disturbed motion of the interface in the disturbance wave region can give rise to the entrainment of small bubbles (Cherdantsev et al [9]) which may penetrate to the more highly superheated zone near the wall and trigger nucleation at existing centers there. However, Barbosa et al [5] argued that nucleation still occurred underneath the disturbance wave region even when no entrained bubbles were observed in their experiments.

In the present paper we propose a new hypothesis to explain why nucleation occurs underneath the disturbance wave. It seems probable that the disturbance waves are turbulent regions separated by laminar substrate regions (Jayanti and Hewitt [4]). The turbulence in the disturbance waves gives rise to a much higher *average* heat transfer coefficient (i.e. a lower average wall temperature) but there is a very important difference between the essentially laminar substrate regions and the turbulent wave regions. This difference is that (for a given heat flux) the wall temperature in the turbulent wave region may fluctuate due to the action of near wall turbulence. The magnitude of the fluctuations may lead to the triggering of nucleation sites in the wave region. These near wall turbulent structures, commonly named *turbulent streaks* are well known to people studying single-phase turbulent thermal boundary layers (Kawamura et al [10]). In the work described here, the influence of near-wall turbulence in the disturbance wave regions of a two-phase annular flow has been explored using CFD methods.

The rest of this paper is organized as follows. In Section 2, we present the details of our model. A discussion of our numerical results is provided in Section 3. Finally, Section 4 is devoted to concluding remarks.

2. Computational model

The work described in present paper used a wall-resolved Large Eddy Simulation (LES) to qualitatively illustrate the idea introduced here. The simulation considered is a single-phase model considering only the liquid region of the annular flow with a fixed sinusoid-type disturbance where interfacial shear is applied to simulate the action of the gas phase not modeled here. This configuration is based on the work of Jayanti and Hewitt [4] where only Reynolds-Averaged Navier-Stokes (RANS)

type simulations were performed. The LES results show that temperature fluctuations yield local hotspots clustered in the frontal part of the wave that are well above the average temperature along the wave and could explain the presence of observed nucleation.

2.1 Problem specification

The general problem definition is a disturbance wave together with the associated upstream and downstream substrate films in an annular flow. The configuration of the wave is based on the work of Jayanti and Hewitt [4]. The interface shape is modelled in a vertical upward annular flow, as shown in Fig. 1. The effect of the gas phase was taken into account by using empirical correlations for interfacial stress (as was done by Jayanti and Hewitt [4]). Note that only the liquid phase was considered in the computations described below. The flow is from the left to the right (against the gravity vector) and the left and right surfaces on the boundary are taken to be periodic planes representing the approximate periodicity of the disturbance waves in streamwise direction. In the azimuthal direction, simulating the entire liquid annulus would yield very high computational costs. Thus, noting that the flow is statistically axisymmetric, only a 20 deg. sector domain of the 3D disturbance wave was adopted herein and the front and back surfaces on the boundary are taken as to be periodic planes accordingly. The size of the sector was chosen to be large enough to have uncorrelated turbulence (see Fig. 1) between the mid-section of the domain and a periodic side. The wall moves at the wave velocity in a direction opposite to the flow so as to keep the interface shape fixed. The flow is driven by the shear stress imposed at the interface, which represents the interaction with the gas phase not simulated here. The dimensions and flow conditions are typical of those occurring in annular flow in which the Reynolds number for gas phase and substrate liquid film are 300 000 and 1670, respectively.

In the present study, a sinusoid wavy interface is adopted and kept fixed throughout the calculations. The only limit of this model is that the wave geometry does not change. This underlying assumption indeed neglects the dynamic evolution of disturbance wave and hence makes the simulation computationally tractable. This is the reason why the present study is only qualitative. The flow field and the temperature field in the flow domain are calculated using the ANSYS Fluent software [11].

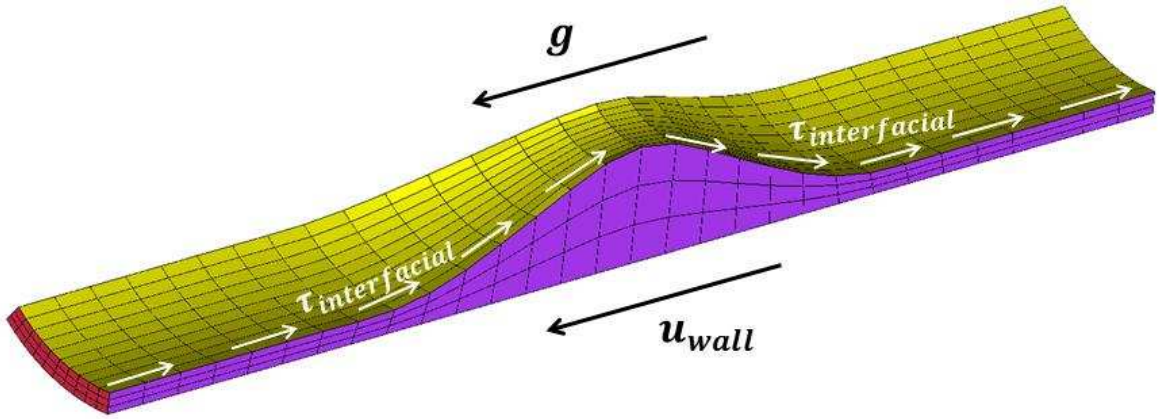

Figure 1 Schematic illustration of the wave/substrate system modelled in the present work. For the sake of clarity, only some grids are drawn and the actual grid is much finer (60×200×700 nodes in *r*-, *θ*- and *z*- directions, respectively) than that shown in the figure.

Prior to the CFD simulation, a two-point correlation on velocity component (definition on correlation coefficient, ρ_{mn}, given in Eq. 1) has been performed to investigate if the current domain is large enough in the circumferential direction.

$$\rho_{mn} = \frac{\overline{u_m(x,t)u_n(x,t)}}{\left[\overline{u_m^2}(x,t)\overline{u_n^2}(x,t)\right]^{1/2}} \qquad m = 0, \quad n = 1,2,\dots\dots 11 \tag{1}$$

where u is the velocity component, m and n are the indexes of velocity probes. x and t indicate the velocity vector and time, respectively.

The location of velocity probes were shown in Figure 2 and two-point velocity correlation coefficient were given in Figure 3. As it can be seen, the turbulence structures are mostly uncorrelated between the two periodic faces, which should allow a correct resolution of the turbulence structures underneath the wave region.

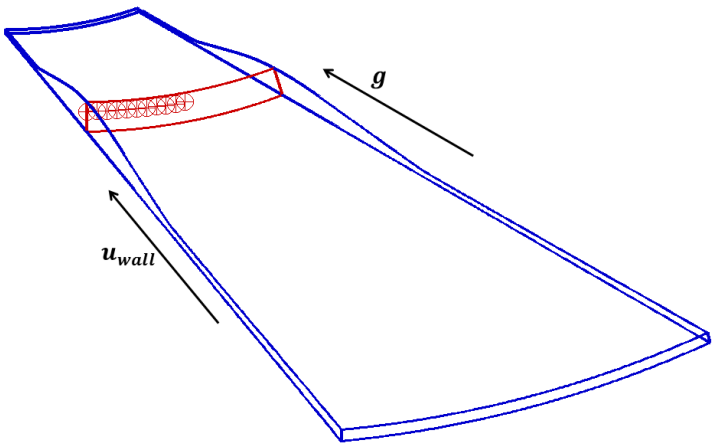

Figure 2 The location of velocity probes for two-point correlation calculation.

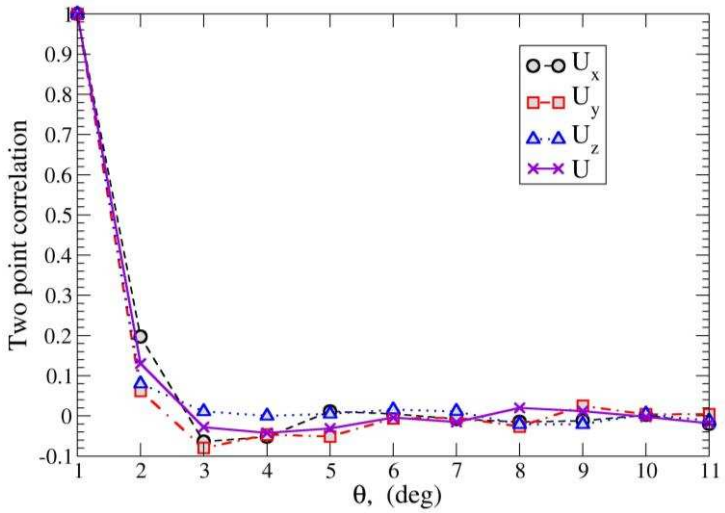

Figure 3 Two point correlation of total velocity and its components x-, y- and z- directions.

2.2 Governing equations

In the Finite Volume Method framework, the governing equations of incompressible pipe flow consist of a single set of continuity, momentum and energy equations. To predict the transient turbulent flow field accurately, a wall resolved LES approach is used. The filtered governing equations solved herein can be written as follows:

$$\frac{\partial \bar{u}_i}{\partial x_i} = 0 \tag{2}$$

$$\frac{\partial \bar{u}_i}{\partial t} + \frac{\partial}{\partial x_j}\left(\bar{u}_i \bar{u}_j\right) = -\frac{1}{\rho}\frac{\partial \bar{p}}{\partial x_i} + \frac{1}{\rho}\frac{\partial \sigma_{ij}}{\partial x_j} - \frac{\partial \tau_{ij}}{\partial x_j} + \boldsymbol{g} \tag{3}$$

$$\frac{\partial \overline{h_s}}{\partial t} + \frac{\partial}{\partial x_i}\left(\bar{u}_i \overline{h_s}\right) - \frac{1}{\rho}\left[\bar{u}_j \frac{\partial \bar{p}}{\partial x_i} - \frac{\partial \bar{p}}{\partial t} - \frac{\partial}{\partial x_i}\left(\lambda \frac{\partial \bar{T}}{\partial x_i}\right)\right] = -\frac{\partial}{\partial x_j}\left[\left(\overline{u_i h_s} - \bar{u}_i \overline{h_s}\right)\right] \tag{4}$$

where ρ and λ are the density and thermal conductivity of the fluid. $\bar{p}$, $\bar{u}$, $\bar{T}$ and $\overline{h_s}$ are the filtered pressure, velocity, temperature and sensible enthalpy field, respectively. $\boldsymbol{g}$ is the gravitational body force. The viscous stress tensor σ_{ij} for incompressible flow is written as

$$\sigma_{ij} \equiv \mu\left(\frac{\partial \bar{u}_i}{\partial x_j} + \frac{\partial \bar{u}_j}{\partial x_i}\right) \tag{5}$$

where μ is molecular viscosity. Subscripts i and j are the vector components in the i-th and j-th directions, respectively.

On the right-hand-side of the filtered momentum equation (Eq. 3), the unknown term,τ_{ij}, is the sub-grid scale stress defined as $\tau_{ij} \equiv \overline{u_i u_j} - \bar{u}_i \bar{u}_j$. In the present case, an eddy viscosity approach was

chosen to the model the sub-grid stress tensor such that $\tau_{ij} = -2\mu_t \bar{S}_{ij}$ with μ_t being the sub-grid scale turbulent viscosity. Here, $\bar{S}_{ij}$ is the rate-of-strain tensor for the resolved scales defined by:

$$\bar{S}_{ij} = \frac{1}{2}\left(\frac{\partial \bar{u}_j}{\partial x_i} + \frac{\partial \bar{u}_i}{\partial x_j}\right) \quad \textbf{(6)}$$

The sub-grid turbulent viscosity is modeled using dynamic Smagorinsky–Lilly model [12] defined as follows:

$$\mu_t = \rho L_s^2 |\bar{S}| = \rho (C_s \Delta)^2 \sqrt{2\bar{S}_{ij}\bar{S}_{ij}} \quad \textbf{(7)}$$

where C_s is the model constant determined dynamically as a function of space and time, and Δ is the local grid size.

In the filtered energy equation (Eq. 4), the term$\left(\overline{u_\iota h_s} - \bar{u}_i \overline{h_s}\right)$, designated the sub-grid enthalpy flux, was modelled by the simple gradient transport hypothesis.

$$\rho\left(\overline{u_\iota h_s} + \bar{u}_i \overline{h_s}\right) = \frac{\mu_t C_p}{Pr_t}\frac{\partial \bar{T}}{\partial x_i} \quad \textbf{(8)}$$

where Pr_t is the sub-grid turbulent Prandtl number (0.85) and C_p is the heat capacity.

In the CFD-based approach used in the simulations reported here, all of the above governing equations are discretized and solved simultaneously using the commercial code ANSYS Fluent ver. 15.0. The pressure-velocity coupling was handled by the Semi-implicit Method for Pressure-linked Equation (SIMPLE) algorithm. A bounded central differencing scheme and a second order upwind scheme were used for the momentum equation and energy equations, respectively. The second order implicit method was used to advance the solution in time.

2.3 Numerical setup

A shear stress, τ_i, varying along the flow direction was imposed on the interface. It's written as

$$\tau_i = \frac{1}{2} f_i \rho_G U_G^2 \quad \textbf{(9)}$$

where $\rho_G$and U_G are the gas density and velocity. The interfacial friction factor, f_i, has different formulation at substrate region [14] and wave region [15], see Eq. 9.

$$f_i \begin{cases} = f_G * \left(0.856 + 0.00281 Re_G \frac{\delta}{D}\right) \text{substrate region, (a)} \\ = \left\{-3.6 \log_{10}\left[\frac{6.9}{Re_G} + \left(\frac{k_{s,d}}{3.7*D}\right)^{1.11}\right]\right\}^{-2} \text{wave region (b)} \end{cases} \quad \textbf{(10)}$$

where f_G is the gas phase friction factor, equals $\frac{0.079}{Re_G^{0.25}}$. Re_G is the gas phase Reynolds number. D is the pipe inner diameter. δ is the local film thickness. $k_{s,d}$ is the equivalent sand roughness that equals to five times the local film thickness [16].

The film thickness δ has the function of

$$\delta(x) = \begin{cases} \frac{1}{2}\left[\left(\delta_{peak} + \delta_{sub}\right) - \left(\delta_{peak} - \delta_{sub}\right)\cos\frac{\pi(x - L_{sub,1})}{L_f}\right], & \text{wave front section} \\ \frac{1}{2}\left[\left(\delta_{peak} + \delta_{sub}\right) - \left(\delta_{peak} - \delta_{sub}\right)\cos\frac{\pi(x - L_{sub,1} - L_f}{L_t}\right], & \text{wave tail section} \\ \delta_{sub}, & \text{substrate region} \end{cases} \quad \textbf{(11)}$$

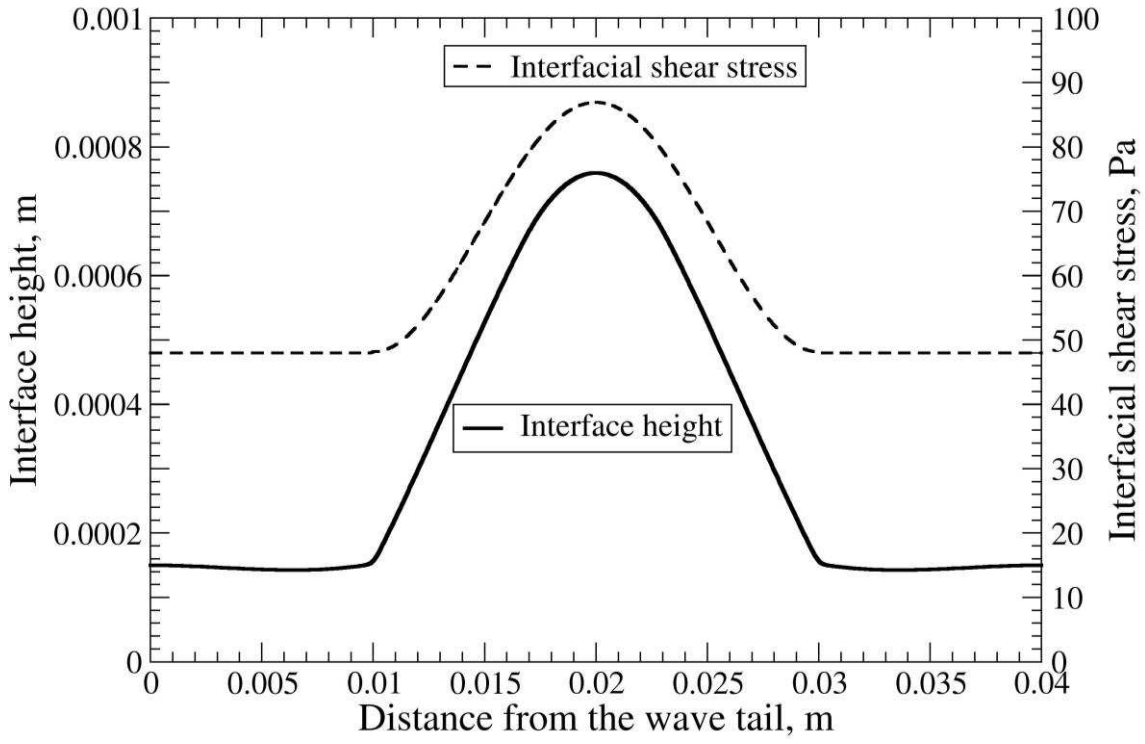

Figure 4 Typical disturbance wave geometry and interfacial shear stress are used for the present work.

A disturbance wave is typically 0.1 m long. To reduce the computational time, the sector mesh 0.1 m long with 0.035 m diameter was selected to mimic the entire wave.

A 3D computational domain, consisting of ~8 million unstructured hexahedral cells, was constructed using the commercial mesh generator ICEM CFD [13]. To resolve the boundary layer adjacent to the wall surface, mesh gradients (fine grids near the wall and coarse grids for the core region) were applied in the radial direction. At the finest mesh point, y^+ <1; this Wall-Resolved Large Eddy Simulation

(WLES) obviates the need to define a wall function. A uniform grid size was used in the axial and circumferential directions. The boundary conditions for the left and right ends were imposed as periodic conditions for WLES simulation in order to take into account the periodicity of disturbance waves. A no-slip condition was imposed on the wall, and a constant wall heat flux (150 kW/m^{-2}) was assumed for the thermal boundary condition. At the interface, a constant temperature, 373.124 K, (a saturation temperature of water at 1 atmospheric pressure condition) was imposed as thermal boundary condition at the vapor-liquid interface.

The LES simulation was initialized from a RANS calculation by adding the fluctuation components which were computed by synthesizing a divergence-free velocity-vector field from the summation of Fourier harmonics. A long enough simulation time (~100s) was adapted herein in order to achieve a statistically fully developed state in terms of velocity and temperature. All of the simulation results (e.g. turbulence, temperature) are collected and analyzed in this run. To ensure accuracy, the global Courant number, *Cr*, was kept to less than 0.5 by choosing a fixed time step of 0.0001s and a maximum number of 20 iterations for each time step (see Eq. 12).

$$C_r = \frac{U\Delta t}{\Delta l} \qquad \text{Eq. 12}$$

where Δl is the dimension of the grid cell at each location and U is the average linear velocity at that location. Δt is the maximum time step size.

3. Modeling Results and Discussion

The aforementioned methodology was used to simulate the flow field under typical air-water annular flow conditions in a 30 mm diameter tube. The results are discussed as below.

A cutting plane sampling the velocity vector in a coordinate frame moving with the wave is shown in Fig. 5. It can be seen that the wall moves from the right to left at the wave velocity, 3m/s. Due to the gas shear acting on the interface, the interfacial velocity is in a direction from left to right and rises to higher value at wave region. The higher interfacial velocity induced by the stronger gas shear eventually results in a chaotic though circulating pattern underneath the wave. This result is consistent with the RANS simulation work by Jayanti and Hewitt [1].

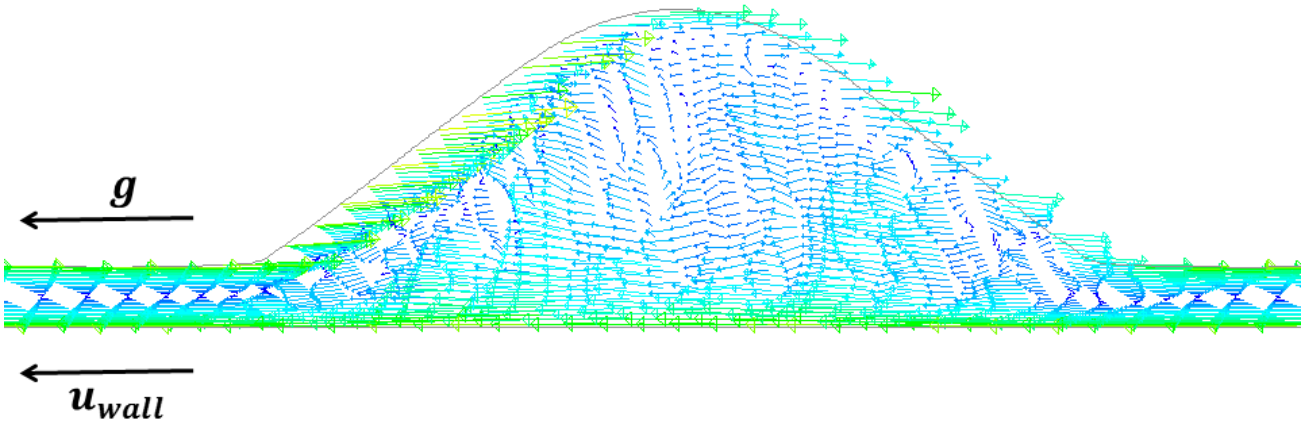

Figure 5 A cut plane samples the velocity vector in a coordinate frame moving with the wave. The contour was foreshortened in horizontal direction for a better view.

The transient wall temperatures have been recorded consecutively and the normalized examples are displayed in Figure 6. As shown, the high temperature region (red color) is formed at the front of wave where the flow just transfers from laminar regime to the slightly turbulent regime. As wave travels forward, these thermal streaks move from wave front towards the wave end.

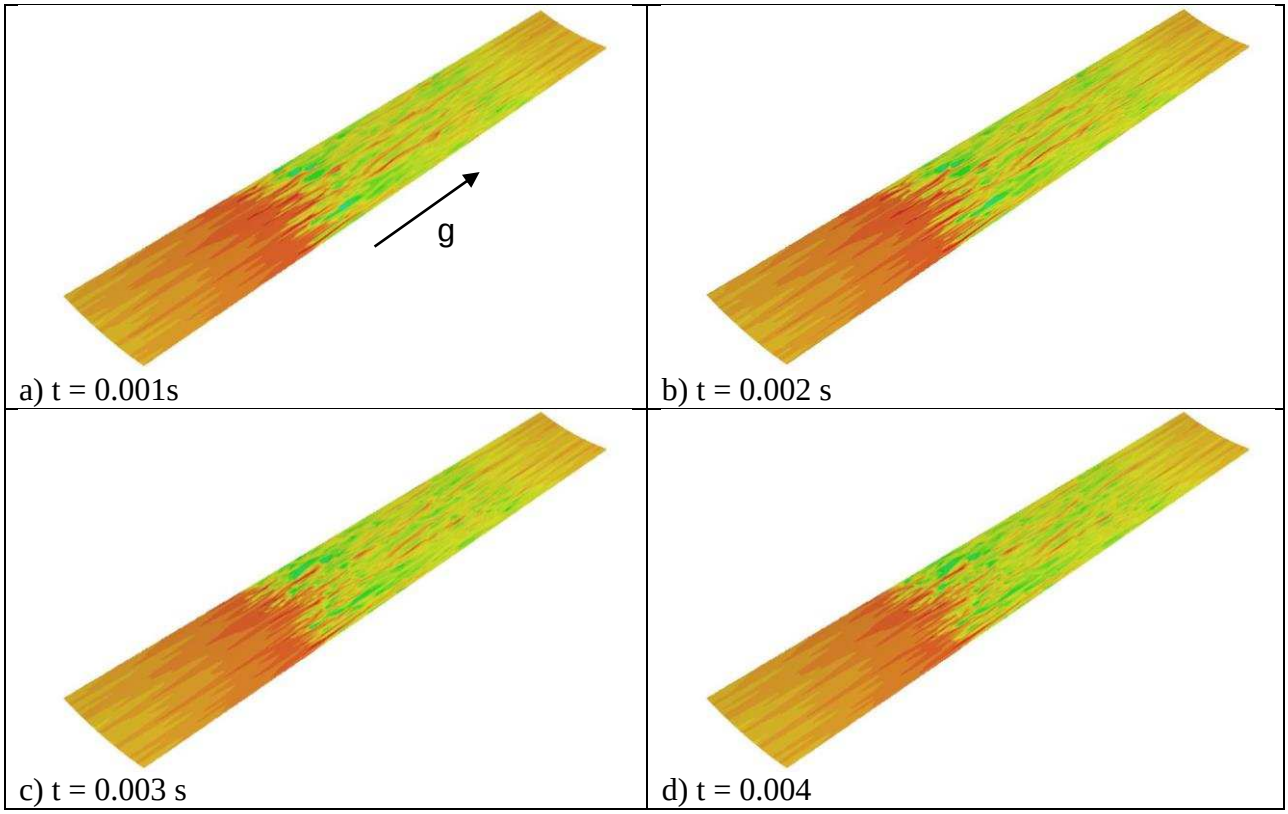

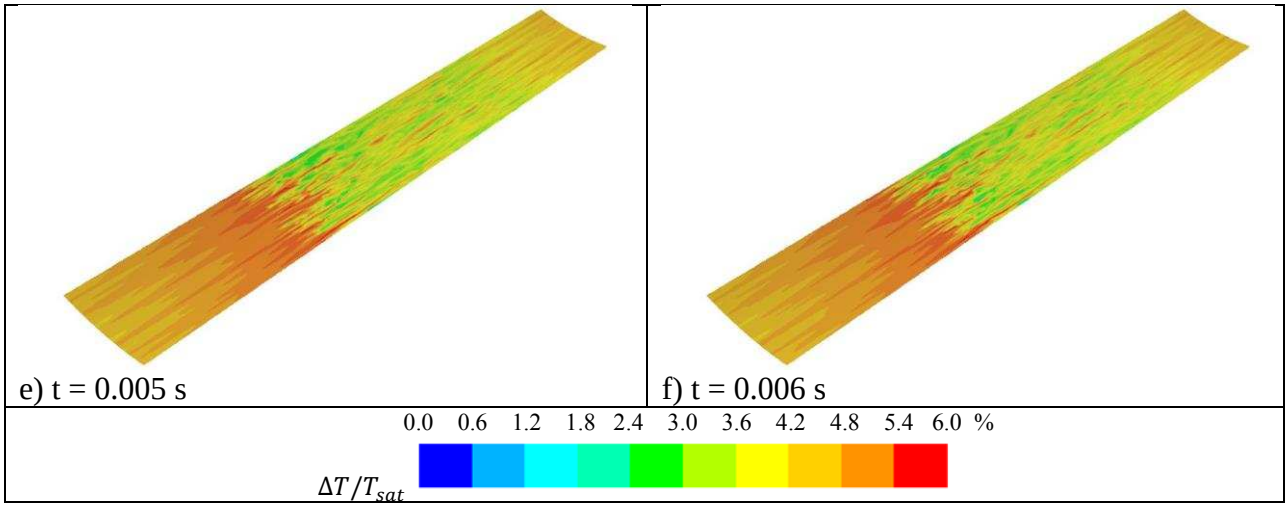

Figure 6 Contour examples of transient wall temperature are recorded consequently, see a)-f) corresponding to time instants starting from 100 s. The time interval between consecutive frames is 1 ms.

To obtain the underlying mechanism of these thermal streaks, the normalized wall temperature fields have been further analyzed using the time average (mean) and root-mean-squares (RMS) of the instantaneous values sampled during the calculation, see Figure 7. The instantaneous wall temperature is time averaged and displayed in Fig 7b. The wall underneath the main wave presents relatively low temperature compared to that in substrate region. However, it also observed a narrow band of high temperature locating at the wave front. This indicates a higher mean heat transfer coefficient for the wave region with a lower HTC for substrate region. The RMS of instantaneous value that reflects the local wall temperature fluctuation is shown in Fig 7c. One can see that the highest temperature fluctuation (up to 6% of T_{sat}) occurs in the wave region due to the turbulence of this region. The large temperature fluctuation induced by velocity streaks in the turbulent flow causes the locally high temperature zone. These locally "hot" spots could trigger the nucleation boiling sites that are induced by the passage of the waves in annular wavy flow as observed in experimental work by Barbosa and Hewitt [5]. On the other hand, the substrate region has small thermal fluctuations, which is consistent with the RANS analysis of Jayanti and Hewitt [4].

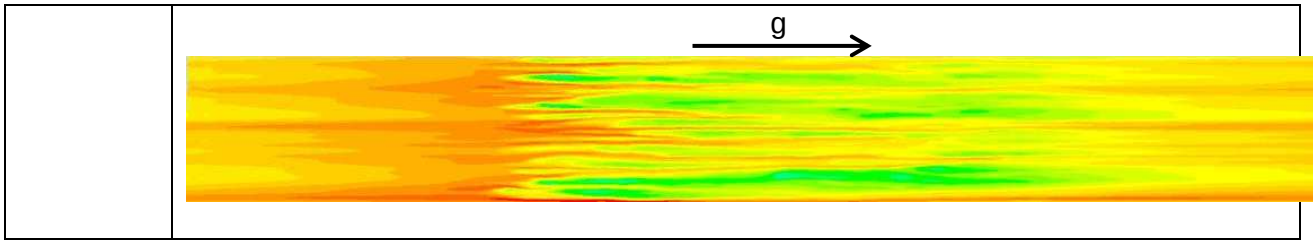

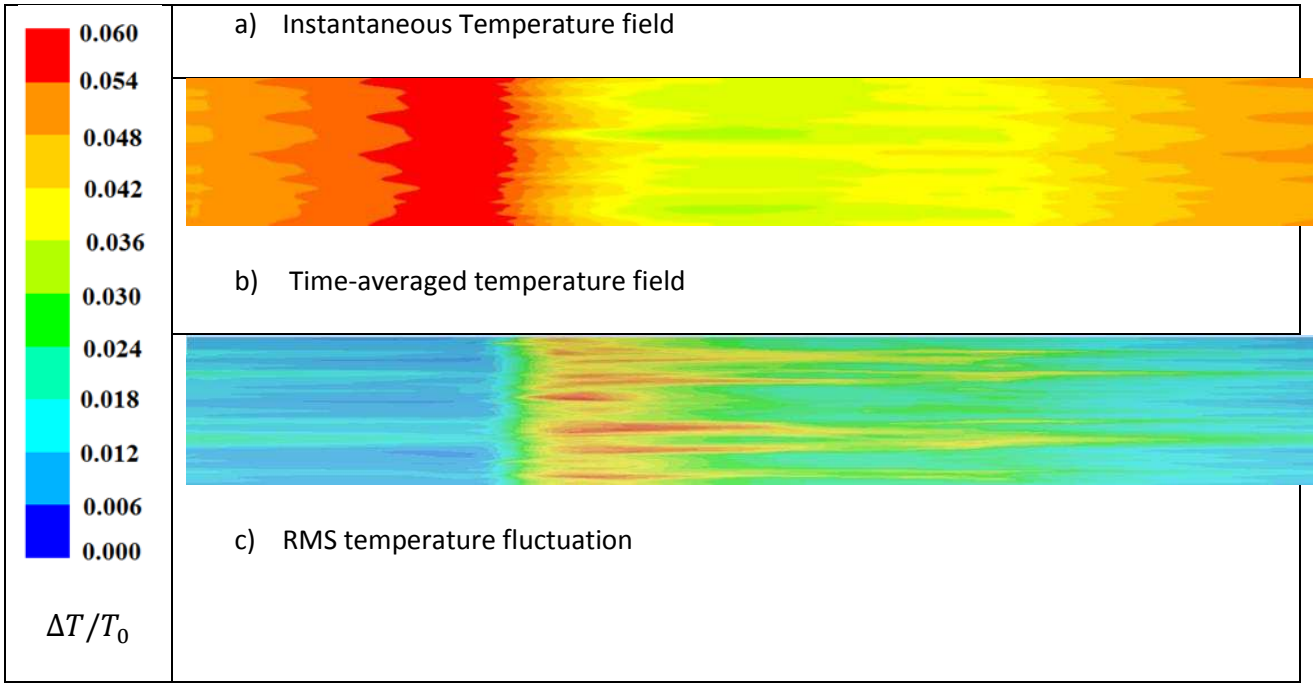

Figure 7 The contours are of normalized temperature, a) instantaneous temperature field, b) time average of temperature field, c) Root-mean-square of temperature fluctuation.

A representation of the computed turbulent structures is shown in figure 8 using iso-surfaces of second invariant of the velocity gradient tensor (i.e. Q-criterion) colored by velocity magnitude. Q-criterion facilitates the visualization on the coherent vortical structure of turbulence. As shown, most vortexes appear underneath the wave where the high temperature fluctuation was observed, whereas, few vortexes were captured in the substrate region. The iso-surface of Q-criterion shows that only the region underneath the wave exhibit turbulent structures whilst the substrate region remains laminar The turbulence in the wave region induces not only the velocity fluctuation, but also the temperature fluctuation, which in turn generates thermal steaks on the pipe wall.

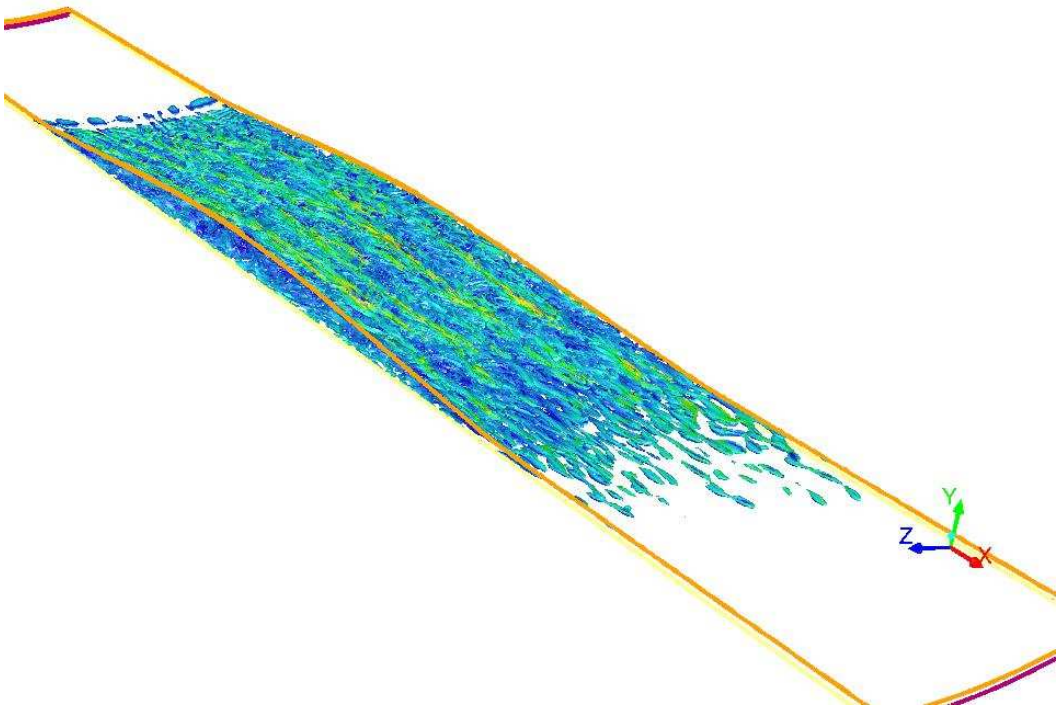

Figure 8 Instantaneous iso-surface of Q-criterion value of flow field

4. Conclusion

In the present work, the flow field in the liquid film under typical annular flow conditions has been studied using a wall resolved LES model. The results show that flow in the substrate region is laminar and turbulent in the wave region, consistent with previous RANS work. In addition, the normalized wall temperature has been recorded and analyzed. It shows although the wave region presents an averaged low temperature, however, locally “hot” spots are formed due to the temperature fluctuation induced by turbulence. These “hot” spots could play a key role in activating of nucleoli boiling sites.

The idea for the calculation being done herein arose from the observation that nucleate boiling was seen (in the experiments [4]) to occur in the disturbance waves. This nucleation is thus seen to be intermittent and it disappears in the ("substrate") regions between the waves. The wave regions present turbulent flow features. For a fixed wall heat flux, these turbulent zones would be expected to have a high heat transfer coefficient and a low average wall temperature compared to the (laminar) substrate zones which would have a higher wall temperature corresponding to a lower heat transfer coefficient value. Thus, the observation of nucleation in the waves seems counter-intuitive. The proposed idea of the present paper is that locally thermal streaks can result in local hot spots that can trigger nucleate boiling in the turbulent region underneath the wave. This hypothesis remains in perfect agreement

with the fact that on average the temperature will be lower underneath the wave and that the heat transfer coefficient will be higher. This hypothesis has been illustrated by carrying out a three dimensional wall resolved large eddy simulation of the disturbance wave treating only the water phase of the annular flow considered.

5. Acknowledgment

This research was performed under the NURESAFE project. The authors wish to acknowledge the EU FP7 for financial support.

6. References

[1] G.F. Hewitt, N.S. Hall-Taylor, Annular two-phase flow, first ed., Pergamon Press, Oxford, 1970.

[2] N.S. Hall-Taylor, G.F. Hewitt, P.M.C. Lacey, The motion and frequency of large disturbance waves in annular two phase flow of air water mixtures, Chemical Engineering Science 18 (1963) 537-552.

[3] G.F. Hewitt, B. Nichols, Film thickness measurement in annular two phase flow using a fluorescence spectrometer technique: Part 2 studies of the shape of disturbance waves, UKAEA Report No. AERE R4506, May 1969.

[4] S. Jayanti, G.F. Hewitt, Hydrodynamics and heat transfer in wavy annular gas-liquid flow: A computational fluid dynamics study, International Journal of Heat and Mass Transfer 40 (1997) 2445-2460.

[5] J.R. Barbosa, G.F. Hewitt, S.M. Richardson, High-speed visualisation of nucleate boiling in vertical annular flow, International Journal of Heat and Mass Transfer 46 (2003) 5153-5160.

[6] ANSYS®Academic Research, Release 15.0, Help System, "ANSYS FLUENT Manual," ANSYS, Inc., 2014.

[7] S. Jayanti, G.F. Hewitt, Response of turbulent flow to abrupt changes in surface roughness and its relevance in horizontal annular flow, Applied Mathematical Modelling 20 (3) (1996) 244-251.

[8] S. Jayanti, T. Kandlbinder, G.F. Hewitt, Turbulent flow in a pipe with intermittent rough patches: An analogue of annular two-phase flow, Chemical Engineering Communications 141-142 (1996) 237-259.

[9] A.V. Cherdantsev, D.B. Hann, B.J. Azzopardi, Study of gas-sheared liquid film in horizontal rectangular duct using high-speed LIF technique: Three-dimensional wavy structure and its relation to liquid entrainment, International Journal of Multiphase Flow 67 (2014) 52–64.

[10] H. Kawamura, K. Ohsaka, H. Abe, K. Yamamoto, DNS of turbulent heat transfer in channel flow with low to medium-high Prandtl number fluid, International Journal of Heat and Fluid Flow 19 (1998) 482-491.